Rapid Communications

Topoelectrical circuit octupole insulator with topologically protected corner states

Jiacheng Bao,[1,*] Deyuan Zou,[2,*] Weixuan Zhang,[2] Wenjing He,[1] Houjun Sun,[1,†] and Xiangdong Zhang[2,‡]

[1]*Beijing Key Laboratory of Millimeter wave and Terahertz Techniques, School of Information and Electronics, Beijing Institute of Technology, Beijing 100081, China*

[2]*Key Laboratory of advanced optoelectronic quantum architecture and measurements of Ministry of Education, Beijing Key Laboratory of Nanophotonics & Ultrafine Optoelectronic Systems, School of Physics, Beijing Institute of Technology, 100081, Beijing, China*

(Received 24 August 2019; published 25 November 2019)

Recent theoretical studies have extended the Berry phase framework to account for higher electric multipole moments; quadrupole and octupole topological phases have been proposed. Although the two-dimensional quantized quadrupole insulators have been demonstrated experimentally, octupole topological phases have not previously been observed experimentally. Here we report on the experimental realization of a classical analog of the octupole topological insulator in the electric circuit system. Three-dimensional topolectrical circuits for realizing such topological phases are constructed experimentally. We observe octupole topological states protected by the topology of the bulk, which are localized at the corners. Our results provide conclusive evidence of a form of robustness against disorder and deformation, which is characteristic of octupole topological insulators. Our study opens a route toward higher-order topological phenomena in three dimensions and paves the way for employing topolectrical circuitry to study complex topological phenomena.

DOI: 10.1103/PhysRevB.100.201406

Topological phases exhibit some very striking phenomena in modern physics. A prominent feature of a topological phase is the emergence of topologically protected edge states, which are robust against local perturbations and play a crucial role in the topological functionality of the underlying system [1–4]. Topological insulators as important platforms for realizing topologically protected boundary states have attracted great attention in recent years [2–5]. They have been constructed in various systems ranging from traditional electronic setups [2–5] to mechanical [6], electromagnetic [7–11], and acoustic [12–14] structures governed by classical wave equations.

Recently, a class of symmetry-protected topological insulators, the higher-order topological insulator, has drawn research interest [15–17]. Unlike conventional first-order topological insulators, two-dimensional (2D) second-order topological insulators have topologically protected corner states, and corresponding 3D systems have topological gapless modes on the hinges. In some crystalline structures, the topological corner and hinge states can arise only from the nontrivial bulk topology when the lattice termination is compatible with the crystal symmetries. The first prediction of a second-order topological insulator, based on quantized quadrupole polarization, was demonstrated in classical mechanical [18] and microwave [19] systems, as well as in electrical circuits [20,21]. The other kinds of second- and third-order topological phases have also been observed in acoustic, photonic, and electronic systems [22–44]. However, the experimental realization of much higher topological insulators, such as octupole topological insulators, remains challenging.

Here we report on the experimental realization of classical analog of octupole topological insulator using 3D topolectrical circuits. The circuits consist of some basic circuit elements: capacitors and inductors, which are constructed experimentally. The octupole topological phases, which are localized at the corners, are observed. The octupole topological insulators that depend only on the bulk topology are demonstrated experimentally.

Theoretical design of topolectrical-circuit octupole insulator. LC circuit models are well suited to the implementation of tight-binding models, because it is possible to establish a correspondence between individual hopping terms in the tight-binding model and individual components in its circuit realization [45–51]. This potential has already been exploited experimentally to implement conventional and quadrupole topological insulators [20,21]. Now, we extend the LC circuit model to study three-dimensional octupole insulator. We consider a 3D circuit unit cell shown in Fig. 1(a), which a tight-binding model with quantized octupole insulator can be constructed by using it.

The unit cell consists of two pairs of capacitors and inductors, (L_1, C_1) and (L_2, C_2), which satisfy the relations $C_2 = \lambda C_1$ and $L_1 = \lambda L_2$. So that they have a same resonance frequency $\omega_0 = (L_1C_1)^{-1/2} = (L_2C_2)^{-1/2}$. Here λ is real positive parameter. The red parts are the groundings in eight sites. It is worth noting that different values of grounded capacitors/inductances should be used to make the on-site potential on each lattice site become zero at the working frequency (see details in Ref. [52]). So sites 1, 2, 3, and 4 are

*These authors contributed equally to this work.

†Author to whom correspondence should be addressed: sunhoujun@bit.edu.cn

‡zhangxd@bit.edu.cn

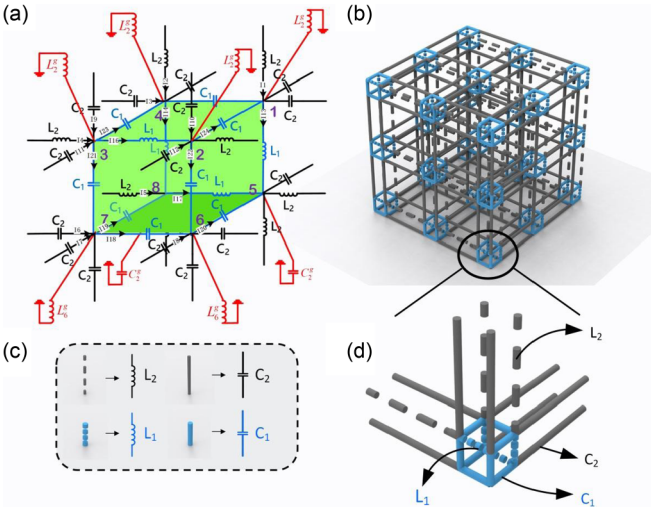

FIG. 1. Circuit model of the octupole topological insulator. (a) Unit cell of the circuit. The capacitors and inductors are marked in the figure. Blue and black circuit elements correspond to weak and strong bonds in a tight-binding or mechanical analog of the circuit. Red circuit elements connect to the ground for the sites 1, 2, 3, 4, 5, 6, 7, and 8 via inductivities and capacitors. (b) Circuit scheme with $3 \times 3 \times 3$ unit cells. (c) the corresponding marks for inductivities and capacitors in Fig. 2(b). (d) Enlarged corner region including a unit cell in (b).

connected to the ground via an inductivity $L_2^g = L_1/(1+\lambda)$, sites 6 and 7 are connected to the ground via an inductivity $L_6^g = L_1/(3+3\lambda)$, sites 5 and 8 are connected to the ground via an capacitor $C_2^g = C_1 + C_2$. So, we can use the parameters ω_0 and λ to describe the topological properties of the circuit unit cell.

In order to realize an octupole insulator with topologically protected corner states, the system should have three anticommuting mirror symmetries [15]. So, the same anticommuting mirror symmetries should also be owned by our classical circuit systems. According to this condition, we build a classical analog of the electric octupole insulator, which has three anticommuting mirror symmetries (M_x, M_y, and M_z) for modes near a specific frequency ω_0. We first consider an infinite periodic structure realized by the above circuit unit cell, and study the bulk properties of the system, before analyzing boundary modes. We then analyze the circuit with periodic boundary conditions in momentum space. In circuit systems, we can derive the circuit Laplacian by the Kirchhoff's current law [45–51],

$$J(\omega) = i\omega C - \frac{i}{\omega} W, \tag{1}$$

where $J(\omega)$ is the circuit Laplacian, and C is capacitance, W is the inverse inductivity $W = L^{-1}$. The off-diagonal components of matrix C are the capacitances C_{ab} between nodes a and b. The diagonal components of matrix C are total node capacitances C_{aa}. The matrix W is the same as C. Under the condition $\omega = \omega_0$, one of the bonds on each square in the green cube shown in Fig. 1(a) has a negative sign, and each square plaque contains π flux in each direction. Using Fourier transform, the circuit Laplacian $J(\omega)$ in Eq. (1) can be transformed to the following $\widetilde{J}_\lambda(\omega_0, q)$ in the momentum space [52]:

$$\begin{aligned}\widetilde{J}_\lambda(\omega_0, q) = i\sqrt{\frac{C_1}{L_1}}[&\lambda \sin q_y \Gamma_1' + (1+\lambda\cos q_y)\Gamma_2' \\ &+ \lambda \sin q_x \Gamma_3' + (1+\lambda\cos q_x)\Gamma_4' \\ &+ \lambda \sin q_z \Gamma_5' + (1+\lambda\cos q_z)\Gamma_6'],\end{aligned} \tag{2}$$

where $\lambda = C_2/C_1$, $q_i (i = x, y, z)$ is the phase of Block wave vector propagating along the x, y, and z directions, respectively. $\Gamma_i' = \sigma_3 \otimes \Gamma_i$ for $I = 0, 1, 2, 3, 4$, and $\Gamma_5' = \sigma_2 \otimes I_{4\times4}$ $\Gamma_6' = i\Gamma_0'\Gamma_1'\Gamma_2'\Gamma_3'\Gamma_4'\Gamma_5'$. Here, $\Gamma_0 = \tau_3\sigma_0$, $\Gamma_k = -\tau_2\sigma_k$, and $\Gamma_4 = \tau_1\sigma_0$, for k = 1, 2, and 3. This circuit Laplacian satisfies

$$\begin{aligned}\widehat{M}_x\widetilde{J}_\lambda(\omega_0, q_x, q_y, q_z)\widehat{M}_x^{-1} &= \widetilde{J}_\lambda(\omega_0, -q_x, q_y, q_z), \\ \widehat{M}_y\widetilde{J}_\lambda(\omega_0, q_x, q_y, q_z)\widehat{M}_y^{-1} &= \widetilde{J}_\lambda(\omega_0, q_x, -q_y, q_z), \\ \widehat{M}_z\widetilde{J}_\lambda(\omega_0, q_x, q_y, q_z)\widehat{M}_z^{-1} &= \widetilde{J}_\lambda(\omega_0, q_x, q_y, -q_z),\end{aligned} \tag{3}$$

where $\widehat{M}_x = \sigma_0 \otimes \sigma_1 \otimes \sigma_3$, $\widehat{M}_y = \sigma_0 \otimes \sigma_1 \otimes \sigma_1$ and $\widehat{M}_z = \sigma_1 \otimes \sigma_3 \otimes \sigma_0$ represent reflection symmetry operators, which obey $\{\widehat{M}_i, \widehat{M}_j\} = 0$ $(i, j = x, y, z$ and $i \neq j)$. Here $\tau_i (i = 1, 2, 3)$ and $\sigma_i (i = 1, 2, 3)$ are Pauli matrices, and τ_0, σ_0 are the 2×2 identity matrices. It is found that besides an overall factor of i, $\widetilde{J}_\lambda(\omega_0, q)$ in our circuit takes exactly the same form as the Bloch Hamiltonian matrix of the octupole insulator introduced in Ref. [14]. So that if $\lambda \neq 1$ the spectrum of $\widetilde{J}_\lambda(\omega_0, q)$ is gapped. When $\lambda > 1$, the circuit is an octupole circuit. If $\lambda < 1$, the circuit is a trivial circuit.

Now, we turn to a circuit with open boundary conditions as shown in Fig. 1(b) to realize topologically protected corner modes. To achieve this, two conditions must be satisfied. The first one is that the symmetries protecting the topological feature can not be broken by the boundary. The second one is that the boundary should not cut through the unit cell. To satisfy the first condition, we let the diagonal elements of $J_\lambda(\omega)$ vanish at the resonance frequency ω_0 to protect the symmetry of the circuit. The diagonal elements of $J_\lambda(\omega)$ are the circuit Laplacian in each site including bulk, surface, edge and corner. So, we fix the circuit elements (capacitor and/or inductor) that connect each site to the ground to meet this condition [52]. For the second condition, we let every corner end at a unit cell to meet it.

With all of the conditions and theories discussed above, we finally construct a topolectrical-circuit octupole insulator shown in Fig. 1(b). We terminate each edge of the circuit with a unit cell. So, the circuit satisfies all the symmetries M_x, M_y, and M_z, and topological corner modes could thus be protected at each corner. To prove the validity of our circuit, we calculate the spectrum of the circuit Laplacian as a function of the driving frequency. In the calculation, the parameters C_1 and C_2 are taken as 1 and 3.3 nF, respectively, and L_1 and L_2 are taken as 3.3 and 1 μH. The results are shown in Fig. 2(a), where an isolated mode clearly crosses the gap. It represents the zero-energy eigenvalue of $J(\omega)$ at $\omega = \omega_0$, which corresponds to the topological corner mode.

Next, we calculate the expected frequency difference between the impedances of the bulk, edge, surface and corner modes. The most natural measurement on a circuit is the

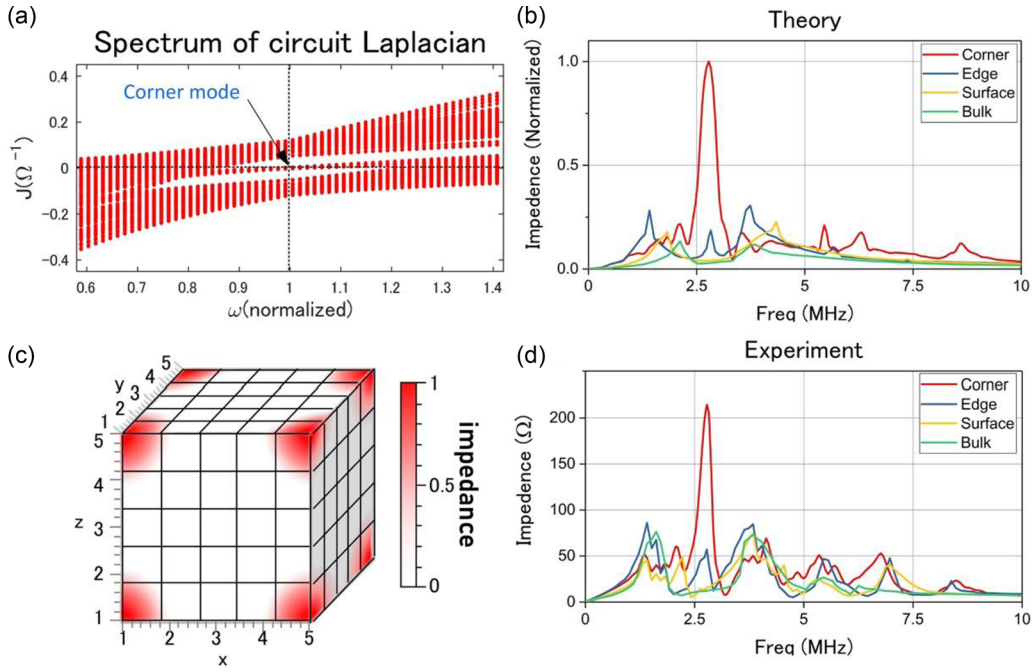

FIG. 2. Comparison of experimental and theoretical results for the circuit spectrum and corner mode. (a) Theoretical spectrum of the circuit Laplacian $J(\omega)$ as a function of the driving frequency. All frequency scales are normalized to the resonance frequency ω_0. An isolated mode crossing the gap, which corresponds to a zero-energy eigenvalue of $J(\omega)$ at $\omega = \omega_0$, is clearly visible. It corresponds to the topological corner mode. The calculation includes a random disorder of 1% for all capacitors and 2% for all inductors. The values of C_1 and C_2 are taken as1 and 3.3 nF, and L_1 and L_2 are taken as 3.3 and 1 μH. (b) Theoretical results of the impedance between two nearest-neighbor sites at the corner, edge, surface, and in the bulk. (c) The distributions of zero-energy eigenvalues for the sample with $3 \times 3 \times 3$ unit cells. (d) Experimental results of the impedance corresponding to (b).

impedance response $Z_{ab}(\omega)$, which is the ratio of the voltage between two nodes a and b due to a current. Mathematically, $Z_{ab}(\omega)$ can be expressed as

$$Z_{ab}(\omega) = G_{aa}(\omega) + G_{bb}(\omega) - G_{ab}(\omega) - G_{ba}(\omega) = \sum_n \frac{|\phi_n(a) - \phi_n(b)|^2}{j_n(\omega)}, \quad (4)$$

where $G_{ab}(\omega) = {J_{ab}}^{-1}(\omega)$ is the circuit Green's function, and $j_n(\omega)$ is the eigenvalue of $J_{ab}(\omega)$, which satisfies $J_{ab}(\omega) = \sum_n j_n(\omega)|\varphi_n(a)\rangle\langle\varphi_n(b)|$. We can see that the impedance can be determined by the smallest eigenvalue $j_n(\omega)$. From the spectrum of circuit Laplacian, we can find that there exist a gap and zero eigenvalue $j_n(\omega) = 0$ in the corner as $\omega = \omega_0$. This phenomenon leads to a large impedance for the corner mode, but not for the other modes. The analysis is agreement with the simulation of the impedance for the circuit. Figure 2(b) shows the simulated result of impedances as a function of the driving frequency. It is seen clearly that the impedance is extremely high for the corner mode as $\omega = \omega_0$, which is different from the low impedances for the bulk, edge, and surface modes. The distributions of zero-energy eigenvalues $j_n(\omega) = 0$ at $\omega = \omega_0$, which correspond to the corner mode, are also plotted in Fig. 2(c). It is shown clearly that strong zero-energy eigenvalues appear at eight corner positions.

The above discussions only focus on the case with a sample size. In fact, we have also calculated impedance responses for the samples of other sizes. With the increase of sample size, similar phenomena can be found. In addition, we have also studied the effect of random capacitors and inductors in the bulk of the sample on the corner modes. Our calculated results show that strong corner modes always appear when the capacitors and inductors vary randomly within the sample or on the surface (except at the corner positions). The most important property of the topologically protected corner state is that it is robust against disorders. We note that the corner state always exists even if the value of used capacitors and inductors on the different positions (except for corners) are randomly varied (the relationships of $C_2/C_1 > 1$ and $L_1/L_2 > 1$ should be satisfied), which is similar to the case in Ref. [15]. In the following, we provide the corresponding experimental results.

Experimental observation of octupole topological phases. In order to observe octupole topological phases experimentally, the circuit with $3.0 \times 3.0 \times 3.0$ unit cells, corresponding to the above theoretical scheme, is designed. Image of the experiment sample is shown in Fig. 3(a). For the convenience of experiment, we cut the total cube in Fig. 1(b) into six sides. We make these sides on three printed circuit boards (PCBs) in order. Capacitors and inductors connect adjacent sides on every site. The different connection ways result in the difference of groundings. Thus, the six sides are divided into two types: A and B. The images of two different sides A and B are shown in Figs. 3(c) and 3(d), respectively. The detailed description is given in Ref. [52]. The fabricated sample has exactly the same construction shown in Fig. 1(b). This can be seen more clearly from Fig. 3(b), which shows enlarged image at a corner

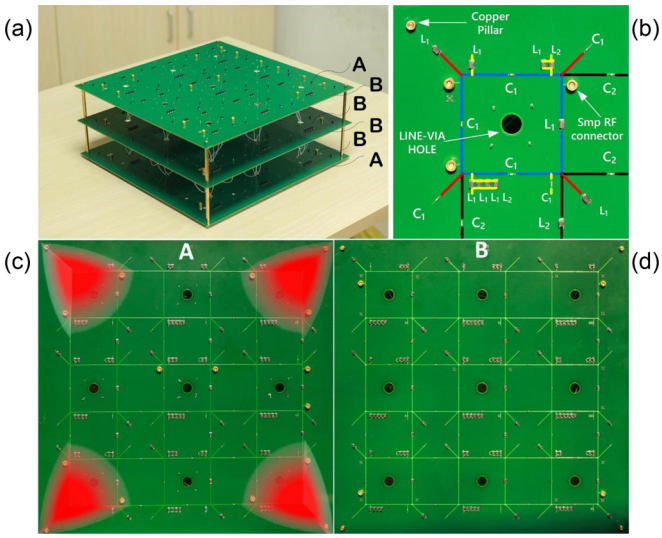

FIG. 3. Experimental sample of the electrical circuit exhibiting topological corner states. (a) Image of the printed circuit board of the octupole topological insulator with three unit cells, corresponding to Fig. 1(b). (b) Enlarged corner region including a unit cell in (a). (c) and (d) show the images of the printed circuit board for two different sides A and B, respectively. The impedance distributions at the frequency ω_0 are also shown.

of the PCB. The blue and black parts in Fig. 3(b) represent the capacitors and inductors on one side. The red parts are the capacitors and inductors connecting adjacent sides. The yellow parts are the capacitors and inductors connecting each site to ground. The line via hole is used to pass wire which connects adjacent sides on different PCB. The Smp connector being located at each site is used for measurement. The copper pillar is connected to ground, which could also support three PCBs.

As for the design of the PCB, all PCB traces have a relatively large width (0.7 mm) to reduce the parasitic inductance of the traces. The spacing between lines is large enough to avoid spurious inductive coupling. The parameters of circuit elements are taken as identical with the above theoretical calculations. The tolerance of the circuit elements is 1%, which can avoid the experiment error. We set $\lambda = C_2/C_1 = L_1/L_2$ to be 3.3, and the resonance frequency to be 2.77 MHz. We used a Wayne Kerr precision impedance analyzer to measure the impedance of the circuit as a function of the driving frequency. The experimental results are shown in Fig. 2(d). The excellent agreement between experimental results and the theoretical predictions have been observed. The theoretical impedance corner peak is normalized to unity, and the experimental impedance corner peak reaches 215 Ω. The red line represents the corner mode, which is extremely high in the resonance frequency. The other lines, which are blue, yellow, and green lines, have a small impedance in resonance frequency. The experimental results for the impedance distributions at the frequency ω_0 are also provided in Figs. 3(c) and 3(d) for sides *A* and *B*, respectively. The red parts in Fig. 3(c) mean the appearance of large impedance in the corner. We can see that only side *A* has red parts but not *B*, which means the large impedance in eight corners, but not in edges, surface, and bulk. This means that our experiment successfully demonstrates the existence of corner states in the octupole topological circuit.

In summary, we have provided experimental evidence of octupole topological phases of matter. Our circuit implementation of the octupole topological insulator has confirmed the existence of the theoretically predicted corner modes and firmly established their origin from the bulk octupole topology. Before this work, only quadrupole topological insulator in 2D has been realized experimentally in many classical systems, such as photonic, phononic, and electronic circuit systems [15–21]. However, the octupole topological insulator in 3D has never been realized due to the difficulty in structural design and sample fabrication. In this work, we first construct the 3D octupole topological circuit, and the associated 0 D corner state has also been observed. Although the extension of tight-binding lattice modal from 2D to 3D seems direct, the actual circuit design is not straightforward, e.g., the value of a grounded capacitor/inductance on different locations (corner, edge, surface, and bulk) should be designed subtly. In this case, our study opens a route toward higher-order topological phenomena in high dimensions and paves the way for employing topolectrical circuit to study complex topological phenomena, offering possibilities to control electrical signals in unprecedented ways.

This work was supported by the National key R & D Program of China under Grant No. 2017YFA0303800 and the National Natural Science Foundation of China (Grants No. 91850205 and No. 61421001).

[1] C. Nayak, S. H. Simon, A.Stern, M. Freedman, and S. Das Sarma, Non-Abelian anyons and topological quantum computation, Rev. Mod. Phys. **80**, 1083 (2008).
[2] M. Z. Hasan and C. L. Kane, *Colloquium*: Topological insulators, Rev. Mod. Phys. **82**, 3045 (2010).
[3] X. L. Qi and S. C. Zhang, Topological insulators and superconductors, Rev. Mod. Phys. **83**, 1057 (2011).
[4] B. A. Bernevig and T. L. Hughes, *Topological Insulators and Topological Superconductors* (Princeton University Press, Princeton, NJ, 2013).
[5] F. D. M. Haldane, Model for a Quantum Hall Effect without Landau Levels: Condensed-Matter Realization of the "Parity Anomaly", Phys. Rev. Lett. **61**, 2015 (1988).
[6] S. D. Huber, Topological mechanics, Nat. Phys. **12**, 621 (2016).
[7] F. D. M. Haldane and S. Raghu, Possible Realization of Directional Optical Waveguides in Photonic Crystals with Broken Time-Reversal Symmetry, Phys. Rev. Lett. **100**, 013904 (2008).
[8] Z. Wang, Y. D. Chong, J. D. Joannopoulos, and M. Soljacic, Observation of unidirectional backscattering-immune topological electromagnetic states, Nature (London) **461**, 772 (2009).

[9] L. Lu, J. D. Joannopoulos, and M. Soljaclc, Topological photonics, Nat. Photon. **8**, 821 (2014).

[10] T. Ozawa, H. M. Price, A. Amo, N. Goldman, M. Hafezi, L. Lu, M. C. Rechtsman, D. Schuster, O. Zilberberg, and L. Carusotto, Topological photonics, Rev. Mod. Phys. **91**, 015006 (2019).

[11] W. Zhang and X. Zhang, Backscattering-Immune Computing of Spatial Differentiation by Non-Reciprocal Plasmonics, Phys. Rev. Applied **11**, 054003 (2019).

[12] V. Peano, C. Brendel, M. Schmidt, and F. Marquardt, Topological Phases of Sound and Light, Phys. Rev. X **5**, 031011 (2015).

[13] Z. J. Yang, F. Gao, X. H. Shi, X. Lin, Z. Gao, Y. D. Chong, and B. L. Zhang, Topological Acoustics, Phys. Rev. Lett. **114**, 114301 (2015).

[14] M. Xiao, G. Ma, Z. Yang, P. Sheng, Z. Q. Zhang, and C. T. Chan, Geometric phase and band inversion in periodic acoustic systems, Nat. Phys. **11**, 240 (2015).

[15] W. A. Benalcazar, B. A. Bernevig, and T. L. Hughes, Quantized electric multipole insulators, Science **357**, 61 (2017).

[16] W. A. Benalcazar, B. A. Bernevig, and T. L. Hughes, Electric multipole moments, topological multipole moment pumping, and chiral hinge states in crystalline insulators, Phys. Rev. B **96**, 245115 (2017).

[17] F. Schindler, A. M. Cook, M. G. Vergniory, Z. J. Wang, S. S. P. Parkin, B. A. Bernevig, and T. Neupert, Higher-order topological insulators, Sci. Adv. **4**, eaat0346 (2018).

[18] M. Serra-Garcia, V. Peri, R. Süsstrunk, O. R. Bilal, T. Larsen, L. G. Villanueva, and S. D. Huber, Observation of a phononic quadrupole topological insulator, Nature (London) **555**, 342 (2018).

[19] C. W. Peterson, W. A. Benalcazar, T. L. Hughes, and G. Bahl, A quantized microwave quadrupole insulator with topologically protected corner states, Nature (London) **555**, 346 (2018).

[20] S. Imhof, C. Berger, F. Bayer, J. Brehm, L. W. Molenkamp, T. Kiessling, F. Schindler, C. H. Lee, M. Greiter, T. Neupert, and R. Thomale, Topolectrical circuit realization of topological corner modes, Nat. Phys. **14**, 925 (2018).

[21] M. Serra-Garcia, R. Süsstrunk, and S. D. Huber, Observation of quadrupole transitions and edge mode topology in an LC circuit network, Phys. Rev. B **99**, 020304 (2019).

[22] H. R. Xue, Y. H. Yang, F. Gao, Y. D. Chong, and B. L. Zhang, Acoustic higher-order topological insulatoron a kagome lattice, Nat. Mater. **18**, 108 (2019).

[23] X. Ni, M. Weiner, A. Alù, and A. B. Khanikaev, Observation of higher-order topological acoustic states protected by generalized chiral symmetry, Nat. Mater. **18**, 113 (2019).

[24] X. J. Zhang, H. X. Wang, Z. K. Lin, Y. Tian, B.Y. Xie, M. H. Lu, Y. F. Chen, and J. H. Jiang, Second-order topology and multidimensional topological transitions in sonic crystals, Nat. Phys. **15**, 582 (2019).

[25] Z. Zhang, M. R. López, Y. Cheng, X. Liu, and J. Christensen, Non-Hermitian Sonic Second-Order Topological Insulator, Phys. Rev. Lett. **122**, 195501 (2019).

[26] H. Fan, B. Xia, L. Tong, S. Zheng, and D. Yu, Elastic Higher-Order Topological Insulator with Topologically Protected Corner States, Phys. Rev. Lett. **122**, 204301 (2019).

[27] H. Xue, Y. Yang, G. Liu, F. Gao, Y. Chong, and B. Zhang, Realization of an Acoustic Third-Order Topological Insulator, Phys. Rev. Lett. **122**, 244301 (2019).

[28] J. Noh, W. A. Benalcazar, S. Huang, M. J. Collins, K. P. Chen, T. L. Hughes, and M. C. Rechtsman, Topological protection of photonic mid-gap defect modes, Nat. Photon. **12**, 408 (2018).

[29] X. Chen, W. Deng, F. Shi, F. Zhao, M. Chen, and J. Dong, Direct Observation of Corner States in Second-Order Topological Photonic Crystal Slabs, Phys. Rev. Lett. **122**, 233902 (2019).

[30] B. Xie, G. Su, H. Wang, H. Su, X. Shen, P. Zhan, M. Lu, Z. Wang, and Y. Chen, Visualization of Higher-Order Topological Insulating Phases in Two-Dimensional Dielectric Photonic Crystals, Phys. Rev. Lett. **122**, 233903 (2019).

[31] F. Schindler, Z. J. Wang, M. G. Vergniory, A. M. Cook, A. Murani, S. Sengupta, A. Y. Kasumov, R. Deblock, S. J. Jeon, I. Drozdov, H. Bouchiat, S. Guéron, A. Yazdani, B. A. Bernevig, and T. Neupert, Higher-order topology in bismuth, Nat. Phys. **14**, 918 (2018).

[32] J. Langbehn, Y. Peng, L. Trifunovic, F. V. Oppen, and P. W. Brouwer, Refection-Symmetric Second-Order Topological Insulators and Superconductors, Phys. Rev. Lett. **119**, 246401 (2017).

[33] Z. Song, Z. Fang, and C. Fang, $(d-2)$-Dimensional Edge States of Rotation Symmetry Protected Topological States, Phys. Rev. Lett. **119**, 246402 (2017).

[34] M. Ezawa, Higher-Order Topological Insulators and Semimetals on the Breathing Kagome and Pyrochlore Lattices, Phys. Rev. Lett. **120**, 026801 (2018).

[35] M. Geier, L. Trifunovic, M. Hoskam, and P. W. Brouwer, Second-order topological insulators and superconductors with an order-two crystalline symmetry, Phys. Rev. B **97**, 205135 (2018).

[36] M. Ezawa, Minimal models for Wannier-type higher-order topological insulators and phosphorene, Phys. Rev. B **98**, 045125 (2018).

[37] E. Khalaf, Higher-order topological insulators and superconductors protected by inversion symmetry, Phys. Rev. B **97**, 205136 (2018).

[38] M. Ezawa, Strong and weak second-order topological insulators with hexagonal symmetry and Z_3 index, Phys. Rev. B **97**, 241402(R) (2018).

[39] E. Cornfeld and A. Chapman, Classification of crystalline topological insulators and superconductors with point group symmetries, Phys. Rev. B **99**, 075105 (2019).

[40] D. Calugaru, V. Juričić, and B. Roy, Higher-order topological phases: A general principle of construction, Phys. Rev. B **99**, 041301 (2019).

[41] M. Ezawa, Non-Hermitian higher-order topological states in nonreciprocal and reciprocal systems with their electric-circuit realization, Phys. Rev. B **99**, 201411 (2019).

[42] T. Liu, Y. Zhang, Q. Ai, Z. P. Gong, K. Kawabata, M. Ueda, and F. Nori, Second-Order Topological Phases in Non-Hermitian Systems, Phys. Rev. Lett. **122**, 076801 (2019).

[43] Y. Xu, Z. Song, Z. Wang, H. Weng, and X. Dai, Higher-Order Topology of the Axion Insulator $EuIn_2As_2$, Phys. Rev. Lett. **122**, 256402 (2019).

[44] W. Zhang and X. Zhang, Photonic quadrupole topological phases in zero-dimensional cavity with synthetic dimensions, arXiv:1906.02967.

[45] J. Ningyuan, C. Owens, A. Sommer, D. Schuster, and J. Simon, Time and Site-Resolved Dynamics in a Topological Circuit, Phys. Rev. X **5**, 021031 (2015).

[46] V. V. Albert, L. I. Glazman, and L. Jiang, Topological Properties of Linear Circuit Lattices, Phys. Rev. Lett. **114**, 173902 (2015).

[47] Y. Hadad, J. C. Soric, A. B. Khanikaev, and A. Alu, Self-induced topological protection in nonlinear circuit arrays, Nat. Electron. **1**, 178 (2018).

[48] C. H. Lee, S. Imhof, C. Berger, F. Bayer, J. Brehm, L. W. Molenkamp, T. Kiessling, and R. Thomale, Topolectrical circuits, Commun. Phys. **1**, 39 (2018).

[49] Y. Lu, N. Jia, L. Su, C. Owens, G. Juzeliūnas, D. I. Schuster, and J. Simon, Probing the Berry curvature and Fermi arcs of a Weyl circuit, Phys. Rev. B **99**, 020302(R) (2019).

[50] T. Helbig, T. Hofmann, C. H. Lee, R. Thomale, S. Imhof, L. W. Molenkamp, and T. Kiessling, Band structure engineering and reconstruction in electric circuit networks, Phys. Rev. B **99**, 161114 (2019).

[51] T. Hofmann, T. Helbig, C. H. Lee, M. Greiter, and R. Thomale, Chiral Voltage Propagation and Calibration in a Topolectrical Chern Circuit, Phys. Rev. Lett. **122**, 247702 (2019).

[52] See Supplemental Material at http://link.aps.org/supplemental/10.1103/PhysRevB.100.201406 for details of (1) Derivation of the circuit Laplacian of the infinite 3D octupole topolectrical circuit in momentum space; (2) The grounding parts at each site of the circuit; (3) The detail for experimental construction of topolectrical-circuit octupole insulator.